Concrete Friction Buffers - Reducing impact from ship collision

Bennedsen, Alexander S. ; Østerby, Isabella ; Nielsen, Lars Lundorf ; Fischer, Gregor; Kleissl, Kenneth; Hoang, Linh Cao

Published in:
Bygningsstatiske Meddelelser

Publication date:
2016

Document Version
Publisher's PDF, also known as Version of record

Årgang LXXXVI, Nr. 1, marts 2016

BYGNINGSSTATISKE MEDDELELSER

udgivet af

DANSK SELSKAB FOR BYGNINGSSTATIK

Proceedings of the Danish Society for Structural Science and Engineering

KØBENHAVN 2016

ISSN 0106-3715 (trykt udgave)
ISSN 1601-6548 (online)

Årgang LXXXVI, Nr. 1. Marts 2016

BYGNINGSSTATISKE MEDDELELSER

udgivet af

DANSK SELSKAB FOR BYGNINGSSTATIK

Proceedings of the Danish Society for Structural Science and Engineering

KØBENHAVN 2016

Artikler offentliggjort i Bygningsstatiske Meddelelser har gennemgået review.

Papers published in the Proceedings of the Danish Society for Structural Science and Engineering have been reviewed.

Concrete Friction Buffers - Reducing impact from ship collision

BYGNINGSSTATISKE MEDDELELSER
Proceedings of the Danish Society for Structural Science and Engineering
Edited and published by the Danish Society for Structural Science and Engineering
Volume 87, No. 1, 2016, pp.1-35

Concrete Friction Buffers - Reducing impact from ship collision

Alexander S. Bennedsen (B.Eng., DTU)
Isabella Østerby (B.Eng., DTU)
Lars Lundorf Nielsen (M.Sc., formerly at COWI)
Gregor Fischer (Ph.D., DTU)
Kenneth Kleissl (Ph.D., COWI)
Linh Cao Hoang (Ph.D., DTU)

1 Introduction

1.1 Motivation

Bridge foundations exposed to the risk of ship collision are often designed to withstand an equivalent static impact force, which has a considerable magnitude. This is a result of the impact force, which is usually determined by assuming the ship to absorb the entire impact energy through plastic deformation [1; 2]. As a consequence, this accidental load case may become governing and lead to larger structural dimensions than needed at the Ultimate Limit State and the Serviceability Limit State.

In reality, the impact energy is only absorbed partly through ship deformation while a significant part may be dissipated by the structure. By taking deformation of the structure into account, a reduced design impact load can be obtained (reductions of more than 50% can be obtained, [3]). This principle is illustrated in Fig. 1

which schematically shows the load-displacement response ($F_{\text{struct.}}$, δ) of the bridge foundation as well as the so-called load indentation curve for the vessel (F_{ship}, x). The sum of the shaded areas below the two graphs represents the amount of energy absorbed during the impact. By consideration of load- and energy balance, we may determine the maximum impact load as well as the required displacement capacity of the foundation structure. When using this design approach and if the structure exceeds its elastic capacity it is necessary to accept permanent deformation of the structure after a ship collision and repair work on the structure is to be expected.

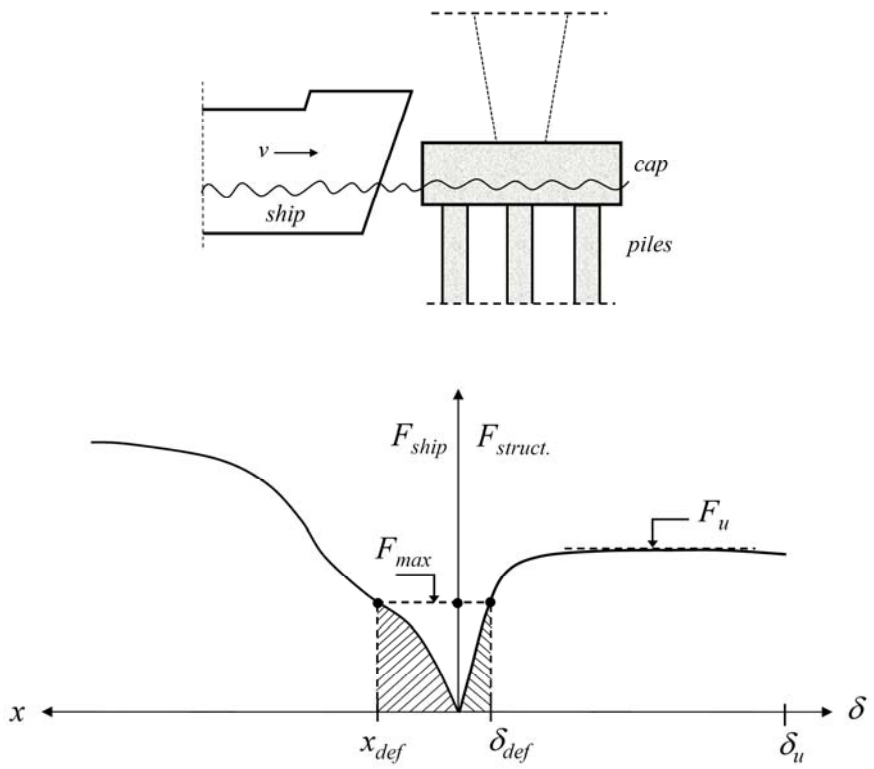

Figure 1: Illustration of ship-foundation collision (top) and illustration of load-deformation response curves for ship and foundation structure (bottom), from [3].

To avoid permanent deformation of the structure, protection systems can be introduced. In that case, the curve representing (F_{struct}, δ) is replaced by the load-displacement response of the protection system. The purpose of this is to let the protection system dissipate the impact energy and at the same time limit the maximum load that can be transferred to the structure. The most common way to protect bridge piers from vessel collision is by underwater constructions [4]. Solutions such as fenders and inflatable floating barriers are also suitable when dealing with relatively small impact energy. For impact from larger vessels with higher

speed and larger collision energy, other systems such as dolphins (sheet piling with concrete cap on top) or artificial islands may be used. These solutions have to be placed at some distance from the bridge foundation and therefore require sufficient space around the perimeter of the foundation. In cases of small crossings and narrow canals many traditional protection systems are not suitable due to the lack of space. Therefore, protection systems installed directly on the foundation structures (e.g. on the pile cap or the pier) may be necessary.

In this paper, we describe the results of an investigation of the mechanical behavior of a new, simple protection system. The system - in the following called Concrete Friction Buffers - is developed by COWI and designed to be installed directly on the foundation structure, e.g. the pile cap. The investigation includes experimental tests as well as modeling and aims to study the load carrying capacity and the displacement capacity of the protection system. The experimental work has been carried out by the primary and secondary author [5][1] under the supervision of the remaining authors.

1.2 Concept of the concrete friction buffer

Fig. 2 schematically shows the principle of the concrete friction buffer protection system. The system consists of a number of (axis symmetrical) conical concrete pistons. The number of pistons to be used depends on the required capacity as well as the magnitude of the impact energy. Each concrete piston is partly encapsulated by a circular reinforced concrete sleeve. The sleeves are reinforced with circular hoops/stirrups and mounted to the pile cap. The interface between sleeve and pile cap has to be designed to enable transfer of contact pressure but at the same time allow free radial expansion of the sleeves at impact. The pistons are connected to a strong front wall (or front diaphragm), which is the structural component that has to transfer the ship impact to all pistons. When a piston (due to ship impact) penetrates through a sleeve, confinement stresses develop and generate friction resistance in the sliding interface between piston and sleeve. Voids in the pile cap at the position of the sleeves allow the pistons to displace without any resistance other than that stemming from friction in the interface to the sleeves. The voids should be equipped with a drainage canal to avoid resistance from entrapped water. The free length of the piston (i.e. the part not encapsulated by the sleeve) and the magnitude of the confinement force are design parameters that control the amount of dissipated energy and the maximum load transferred to the structure. The system is sacrificial and hence, after a ship impact, the system is not repairable and will have to be replaced (i.e. front wall, pistons and sleeves).

[1] Compared to [5], corrections of some minor errors have been made when writing this paper.

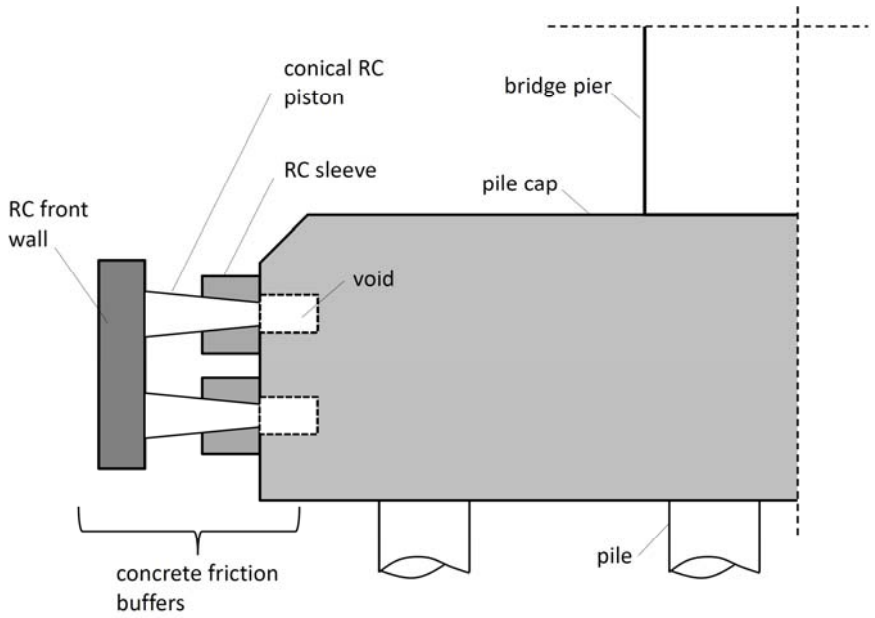

Figure 2: Principle of the concrete friction buffer system for protection of bridge foundations against ship collision.

Fig. 3 illustrates a conical piston partly encapsulated by a sleeve. The system is here shown vertically corresponding to the laboratory test setup. When the load, P, is applied, the piston moves downwards and creates an expansion of the sleeve (corresponding to a change in radius, ΔR, due to the conical shape). The expansion results in development of a confining pressure at the interface between piston and sleeve (in the following also referred to as a clamping force). Initially, the sleeve is un-cracked and the clamping force is caused by tensile normal stresses developed in the concrete in the tangential direction of the sleeve. Then, as the piston continues to penetrate the sleeve, cracks in the radial direction emerge. Subsequently, the contribution from the concrete to the clamping force decreases due to tensile softening and eventually vanishes when the cracks are stress free. Hereafter, only the steel hoop reinforcement contributes to the clamping force. The maximum clamping force that can be developed is a function of the hoop reinforcement ratio and the ultimate strength of the hoops. Once the hoops yield, the piston will displace at almost constant load (i.e. the load bearing capacity of the buffer). The displacement of the piston at constant load may continue until the sleeve has expanded to such an extent, that rupture of the hoops takes place. The displacement capacity depends on the ductility of the hoop reinforcement and the shape of the conical piston (i.e. the inclination of the piston's generatrix).

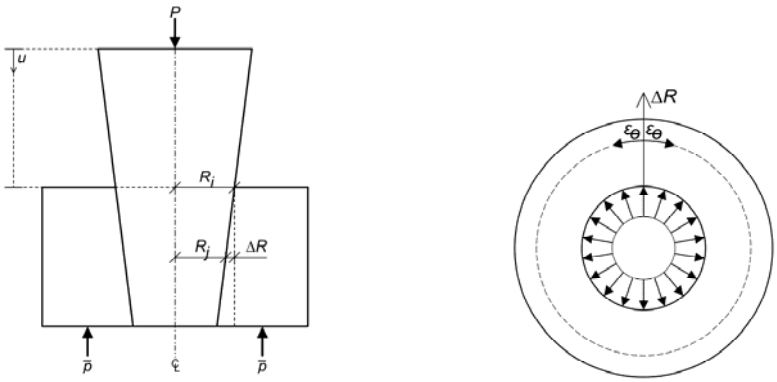

Figure 3: Schematic layout of a concrete buffer consisting of piston and sleeve (left) and illustration of clamping stresses at interface between piston and sleeve (right)

1.3 Design philosophy

When designing a structure for an accidental limit state the material properties (and other relevant properties such as e.g. friction coefficient) are usually defined as a lower bound value typically given by the characteristic 5% fractile. However, for the design of a buffer element, such as those considered here, two sets of properties are necessary to consider; a lower and an upper bound.

To verify that the buffer element is able to absorb the amount of energy applied through impact, the lower bound properties have to be used. This will insure that even when the properties take their worst possible value (lower 5% fractile) the energy absorption is still sufficient. On the other hand, when estimating the maximum force transferred from the buffer element to the foundation structure, it is necessary to adopt the upper bound values for the material properties (upper 95% fractile).

2 Experimental program

2.1 Specimen geometry and material data

In total, ten downscaled test specimens were produced and tested. However, only six specimens had conical piston. The remaining four specimens were with cylindrical pistons. The behavior of these four specimens was distinctly different from that of the specimens with conical pistons. The reason is the lack of radial expansion of the sleeves due to the cylindrical shape. In the following, only test and modelling of the buffers with conical pistons are described.

An overview of the different types of components used in the experimental program can be seen in Fig. 4. The pistons were cast in smooth metal formwork in

order to obtain a smooth surface. After hardening, a sleeve was cast around the pistons (see photos in Fig. 5 showing formwork and reinforcement of sleeve). In practical applications, the buffers may be submerged in water. This means that algae growth will most likely occur. To simulate this situation and to get an estimate of the lowest possible friction at the concrete-concrete interface, wax was applied on the surface of two of the pistons before casting of the sleeve. This should lead to a reduced friction between piston and sleeve as would be expected in practice due to algae growth (the wax was applied to the full length of the pistons even though the section surrounded by the sleeve will not be exposed).

As illustrated in Fig. 4, the concrete buffer (i.e. piston with sleeve) was placed on top of a base. The base was a hollow, reinforced concrete cylinder used as the support of the buffer in the experimental setup up and allows the piston to penetrate through the sleeve. An overview of the six tested buffers can be seen in Table 1. The detailed design of the components is described in the following.

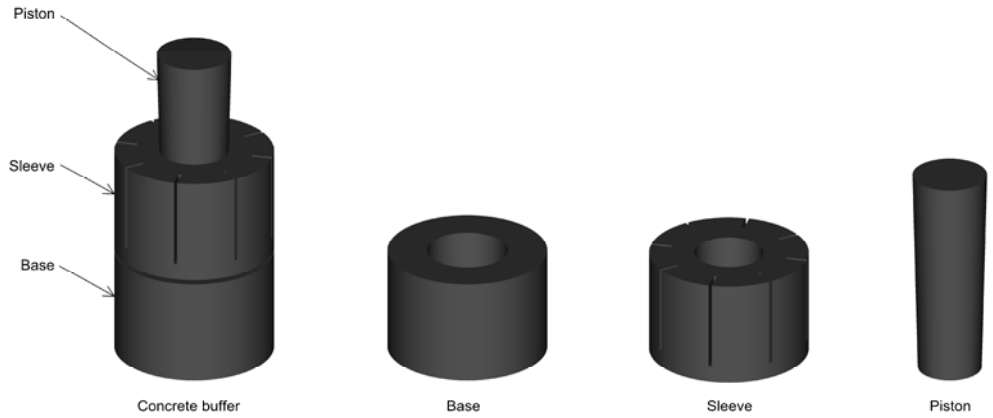

Figure 4: Components of the down-scaled concrete friction buffer (the base is a part of the test setup)

Table 1: Overview of test specimens

Specimen ID.	**Interface property between piston and sleeve**	**Stirrup/hoop content in sleeve*)**
1-L-D	Sleeve cast against *dry* piston surface	Low
2-L-D	Sleeve cast against *dry* piston surface	Low
3-L-W	Sleeve cast against piston surface treated with *wax*	Low
4-H-D	Sleeve cast against *dry* piston surface	High
5-H-D	Sleeve cast against *dry* piston surface	High
6-H-W	Sleeve cast against piston surface treated with *wax*	High

*) High: 10 x Ø12mm stirrups, D = 550 mm *plus* 4 x Ø12mm stirrups, D = 700 mm.
Low: 8 x Ø10 mm stirrups, D = 550 mm *plus* 2 x Ø10 mm stirrups, D = 700 mm.

Figure 5: Piston, stirrups and crack inducers placed within sleeve formwork (left) and buffer system after casting of sleeve (right)

2.1.1 Layout of conical pistons

The pistons had a height of 1 meter. The cross sectional diameter was 350 mm at top and 300 mm at bottom, i.e. a surface inclination of $\tan\alpha$ = 1:40. The pistons were cast with a Class C40/50 concrete and reinforced with Class B ribbed rebars. The layout can be seen in Fig. 6. A steel plate was cast in the top of the piston for load transfer from the testing machine.

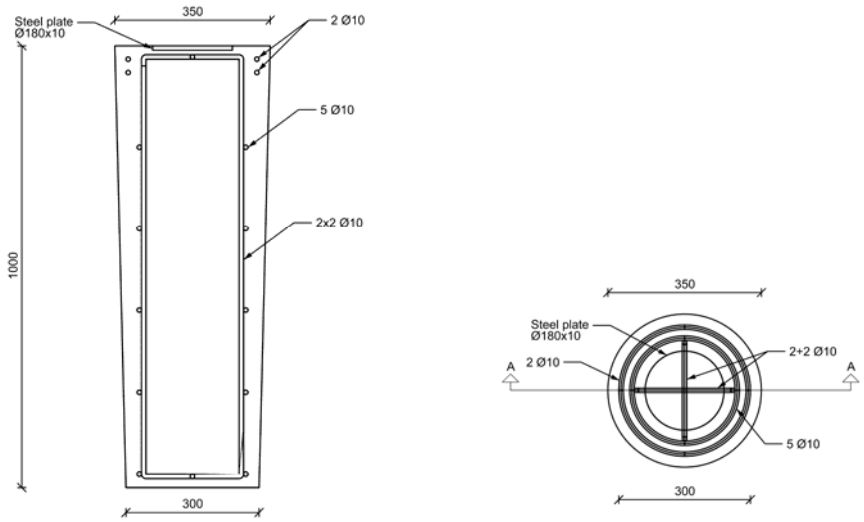

Figure 6: Longitudinal and cross sectional view of piston geometry and location of reinforcement

2.1.2 Layout of sleeves

The sleeves were cast in cylindrical forms with an outer diameter of 750 mm and high of 500 mm (see Fig. 5). The wall thickness of the sleeves varied from 200 mm at the top to 225 mm at the bottom. The effective wall thickness, however,

was smaller for most part of the sleeve. In order to prevent the sleeve wall from being under reinforced (i.e. preventing the tensile capacity of the concrete wall to be larger than the tensile capacity of all stirrups) eight crack inducers were cast into the sleeve. The crack inducers were made of 20mm plywood sheet and reduced the wall thickness by 100 mm in most part of the sleeve. At the bottom, where the sleeves in the experimental setup must be supported by the base, the full thickness of 225 mm was maintained. The positions of the crack inducers can be seen in Fig. 7 (bottom) and the shape of the crack inducers has been indicated by the hatched area in Fig. 7 (top), leaving the un-hatched areas as the effective wall area. The sleeves were provided with circular stirrups (hoops). In three of the sleeves, the stirrups were made from Ø10mm rebars while in the remaining three sleeves, Ø12mm rebars were used. The amount of stirrups per sleeve has been indicated in Table 1. The content of stirrups in the sleeves will in the following be termed high (H) in case of Ø12mm rebars and low (L) in case of Ø10mm rebars. It should be noted that the stirrups had different outer (bend) diameters, D, depending on their position in the sleeve as indicated in Figure 7. In the part of the sleeve where crack inducers reduced the wall thickness, the outer diameter of the stirrups was D = 550mm while in the lower part with thickness 225 mm, the outer diameter of stirrups was D = 700 (see also Table 1).

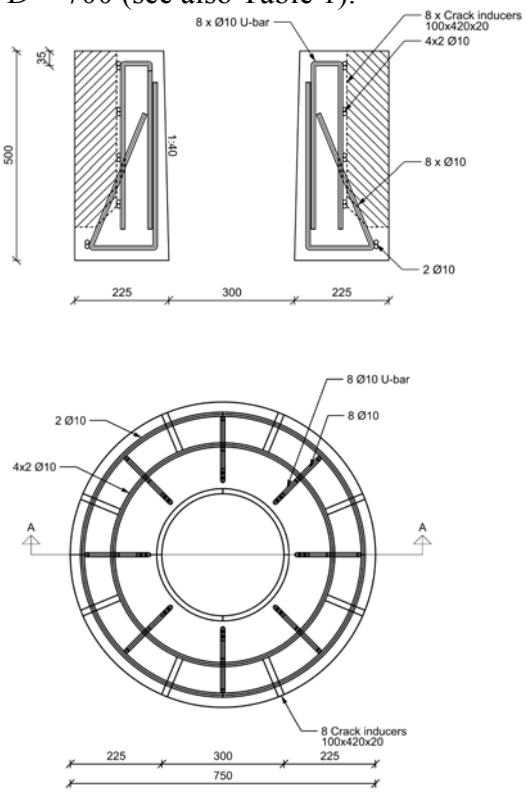

Figure 7: Effective wall thickness of sleeve (top) and position of the eight crack inducers (bottom), reinforcement shown for specimens with low stirrup content.

2.1.3 Properties of reinforcement

Fig. 8 shows a representative stress-strain relationship determined from 10 tensile tests of the Ø10mm and Ø12mm rebars. The rebars used did not have a distinct yield plateau. Therefore, the *0.2%* - stress as well as the ultimate strength f_u has been determined. It should be noted that in the analysis, an idealized elasto-plastic stress-strain relationship will be adopted, where $f_y = f_u$ is assumed. Table 2 summarizes the average values of the main properties needed for modelling in this paper.

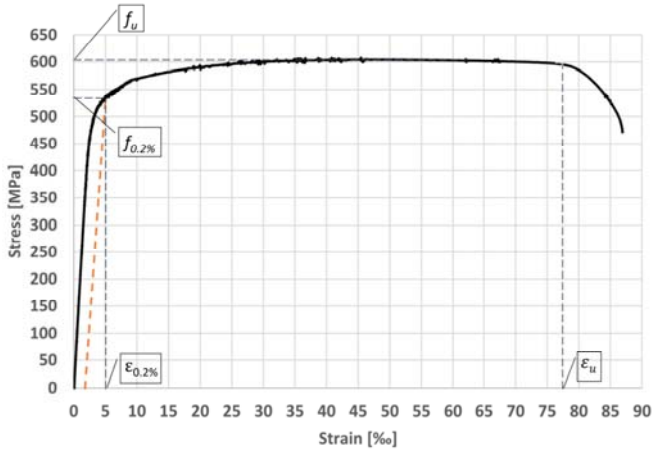

Figure 8: Tested uniaxial stress-strain relationship for Ø10 mm rebars.

Table 2: Reinforcement properties, average values.

Tensile strength f_u [MPa]	**Strain capacity** ε_u [%]	**E-modulus** E_s [GPa]
606.2	7.75	195.5

2.1.4 Properties of concrete

The test specimens were cast at a precast concrete plant using one of the available standard concrete mixtures with maximum aggregate size of 8 mm. (details of the mixture composition may be found in [5]). The uniaxial compressive strength was determined from tests on cylinders cured under the same condition as the buffer specimens. Cylinder compression tests were carried out before, during as well as after testing of the buffers. The results are summarized in Table 3, showing a slight strength increase from 28 days of age to 79 days of age.

Table 3: Average values of tested compressive cylinder strength.

Compressive strength f_c [MPa]	**Age** [Days]	**Period**
48.1	28	(before test of buffers)
52.1	63	(during test of buffers)
54.5	79	(after test of all buffers)

2.2 Test setup

The buffers were tested in a 5 MN INSTRON machine using displacement control. The test setup is schematically shown in Fig. 9 and photo of a specimen in the testing machine is shown in Fig. 10. During the test, displacement of the piston as well as radial expansion of the sleeve was monitored by LVDTs placed as indicated in Figs. 9 and 10. Sixteen "sandwiches" of steel plates with grease in between were placed on the top of the base to support the sleeve (Fig. 11). Support in the form of steel plate "sandwiches" was chosen to allow for unrestrained radial movement of the eight segments of the sleeve that was expected to form due to the crack inducers.

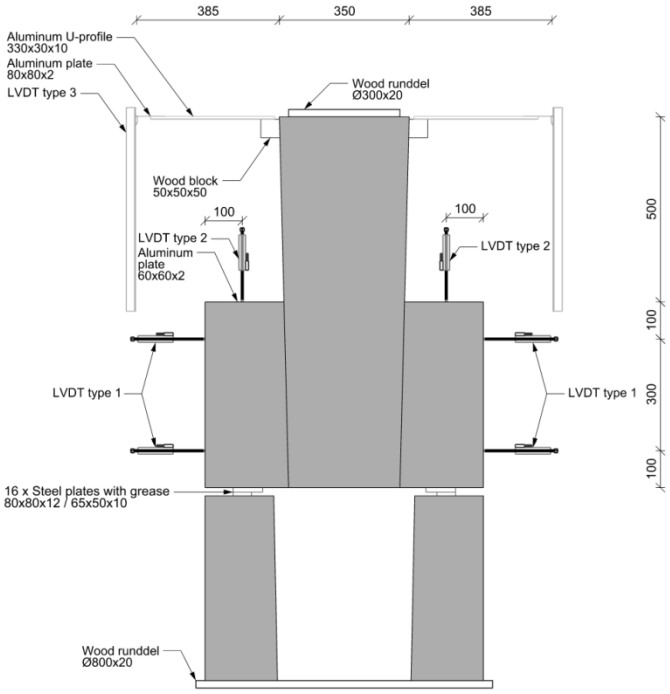

Figure 9: Illustration of test setup with position of LVDTs for displacement measurements.

Figure 10: Test specimen on concrete base placed in 5 MN INSTRON machine.

Figure 11: Sandwiches of steel plates with grease in between placed on top of the concrete base for support of the sleeve.

2.3 Test results

2.3.1 Specimens with low stirrup content in sleeve

Fig. 12 shows the relationship between the applied load, *P*, and downward displacement of the piston, *u*, for test specimen 1-L-D. The following characteristic phases (also indicated in Fig. 12) on the response curve may be identified.

- Crack appearance: Within the first few millimeters of piston displacement, the sleeve cracked at the position of the crack inducers. Before crack appearance, the load-displacement response behavior is very stiff. A significant difference in the stiffness of the buffer is seen prior to and just after cracking. The dis-

placement of the piston after cracking of the sleeve was accompanied by lateral (radial) movement of the segments of sleeve.

- Yielding of stirrups: After crack appearance, the load-displacement response increases almost linearly until a plateau is reached. This happens at about 85% of the maximum load and is due to initiation of yielding in the stirrups.

- Maximum load: A horizontal plateau with maximum load of 2683 kN was observed between appr. 100 mm piston displacement to about 200 mm piston displacement.

- Rupture of stirrups: At about 200 mm piston displacement, the first stirrup(s) ruptured resulting in a vertical drop on the response curve. Thereafter, a sequence of stirrup ruptures occurred resulting in a further drop of load in the response curve.

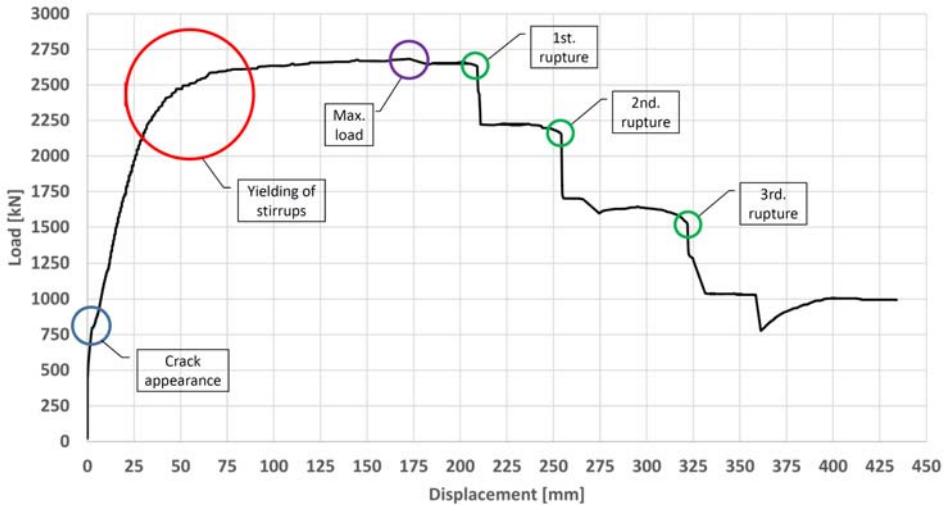

Figure 12: Load vs. piston displacement for specimen 1-L-D (Yield plateau replaced by Yielding of stirrups)

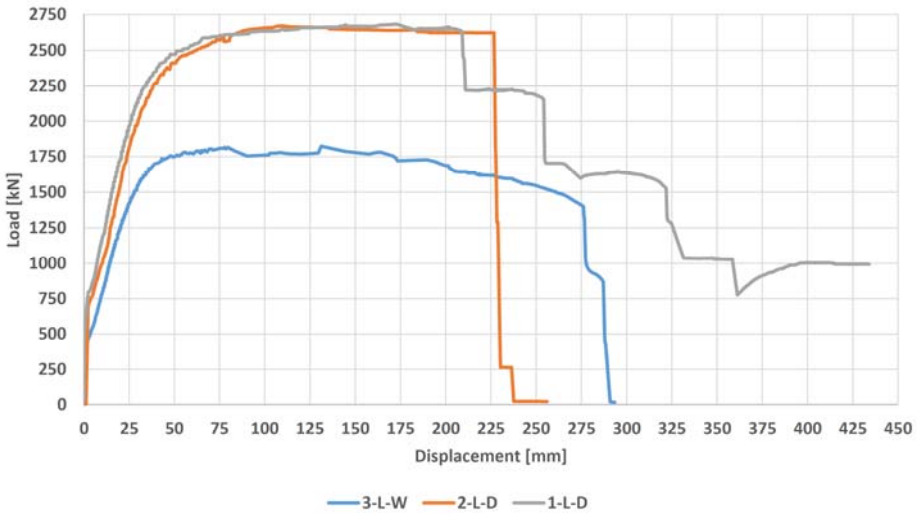

Figure 13: Load vs. piston displacement for all specimens with low stirrup content.

Table 4: Summary of test results for specimens with low stirrup content.

Specimen:	3-L-W	2-L-D	1-L-D
Crack appearance			
Load (kN) Displacement (mm)	462 2.4	696 2.3	796 2.4
Initiation of yielding of stirrups			
Load (kN) Displacement (mm)	1661 37	2261 39	2271 36
Ultimate load			
Load (kN)	1858	2670	2683

The load-displacement responses of all three specimens with low stirrup content are compared in Fig.13 and the main results are summarized in Table 4. As expected, very similar responses are observed for the two identical specimens, 1-L-D and 2-L-D. For these two specimens, there is, however, a difference in the post-peak behavior. While rupture of stirrups (and thereby drop in the response curve) took place one by one in the case of 1-L-D, then nearly all stirrups ruptured at the same time for specimen 2-L-D. This difference may possibly be explained by the locations of the laps of the circular hoops. As shown in Fig. 14, the laps in specimen 1-L-D are more or less randomly located, whereas the laps in specimen 2-L-D have coincidently been placed at the same vertical section. Photos of specimen 2-L-D after testing (see Fig. 15) show cracks pattern and position of stirrup rupture.

From Fig. 13, it can be seen that specimen 3-L-W had a much smaller load carrying capacity than specimen 1-D-L and 2-D-L. This result was expected because

the interface between sleeve and piston in specimen 3-D-W was, as mentioned above, treated with wax to simulate algae growth in practice. This has resulted in a reduced friction in the interface and thus a reduced clamping force and thereby a reduced load carrying capacity.

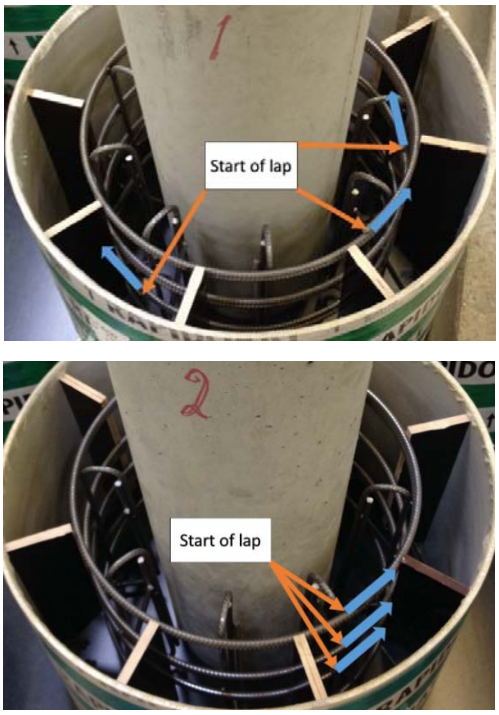

Figure 14: Location of lap for different stirrups in specimen 1-L-D (top) and specimen 2-L-D (bottom).

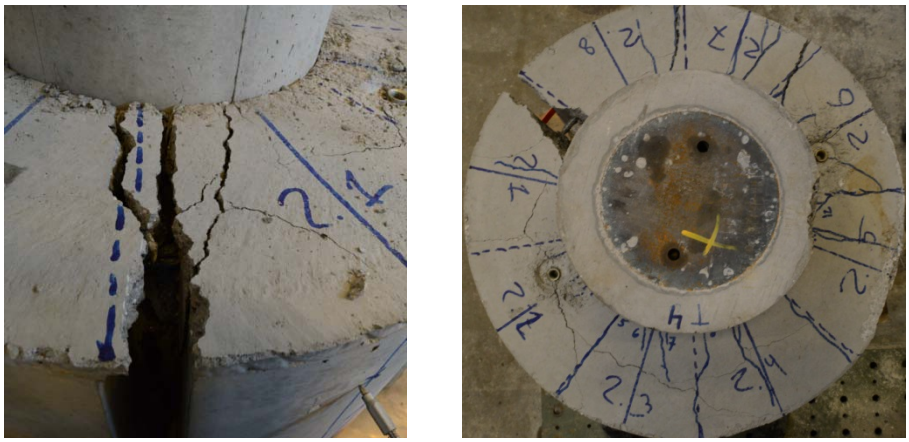

Figure 15: Crack patterns and location of stirrup rupture in sleeve, top view of specimen 2-L-D.

2.3.2 Specimens with high stirrup content in sleeve

The obtained load-displacement responses for specimen 4-H-D, 5-H-D and 6-H-W are shown in Fig. 16. The load at which cracking of the sleeve took place was *785 kN* and *519 kN* for specimens 5-H-D and 6-H-W, respectively. This is comparable to the cracking load levels observed for specimens without and with wax treatment and having a low content of stirrups. The cracking load for specimen 4-H-D is seen to be significantly higher than in the other specimens. In addition, it can be seen that there is a small drop in the response curve just after crack appearance before the load catches up again. This might be the effect of an initial cohesive resistance.

As can be seen, the response curve of specimen 6-H-W (interface wax treated) reached a horizontal plateau (approximately at 3780 kN) with yielding of the stirrups. Displacement measurements with LVDTs only exists up to ca. 70mm for this test. Due to observation of fracture of the sleeve, the LVDTs were removed to avoid damage of testing equipment. The test was, however, carried out to the end (i.e. nearly full penetration of piston). Fig. 17(right) shows the damaged sleeve after end testing for specimen 6-H-W.

For specimens 4-H-D and 5-H-D, it was necessary to terminate the experiment when the stirrups were still behaving elastically (the response curves still show positive gradient at the point of termination). The combination of dry interface and high stirrup content lead to very high clamping forces and resulted in premature crushing of the piston head, see Fig. 17(left).
Hence, the test results for specimens 4-H-D and 5-H-D cannot be used for further study; except perhaps as a warning that when designing the piston, the compressive stress should be limited (at failure, the compressive stress in the two pistons had reached 53 MPa and 62 MPa, respectively) or higher strength concrete should be used to avoid a situation in practice, where the piston becomes the weak link of the concrete buffer system.

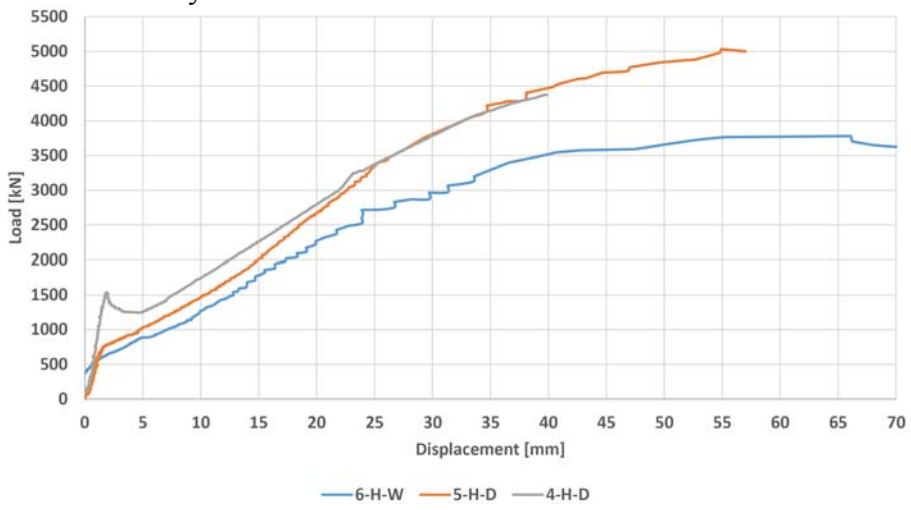

Figure 16: Load vs. piston displacement for specimens with high stirrup content

Figure 17: Crushing of piston before yielding of stirrups in sleeve of specimen 5-H-D (top) and damages of sleeve in specimen 6-H-W after ca. 480 mm piston displacement (bottom)

3 Modelling of load-displacement response

In this section, a simple model for the load-displacement response of the concrete friction buffer is established. The model is used to compare with test results as well as to carry out design optimization in order to obtain as large a displacement capacity as possible for a given geometry and stirrup content.

3.1 Geometry and kinematical relations

Fig. 18 shows a longitudinal section through piston and sleeve. P is the applied load and the reaction at the bottom of the sleeve is considered as a line load $\overline{p}$. The displacement of the piston is denoted u and the conical shape of the piston is described by the angle of the generatrix, α. The initial inner radius (i.e. geometry before loading) of the sleeve is $R(z)$, where $z = 0$ corresponds to the top face of the sleeve and $z = h$ corresponds to the bottom face of the sleeve. As indicated, the initial radii are $R(z = 0) = R_0$ and $R(z = h) = R_1$. In addition, R_{s1} describes the initial radius of the stirrups placed in the portion of the sleeve with a reduced effective wall thickness (due to the crack inducers) and R_{s2} is the initial radius of the stirrups placed at the bottom of the sleeve where there is no reduction of wall thickness (For the test specimens, R_{s1}= 550/2 = 225 mm and R_{s2} = 700/2 = 350 mm, cf. Table 1).

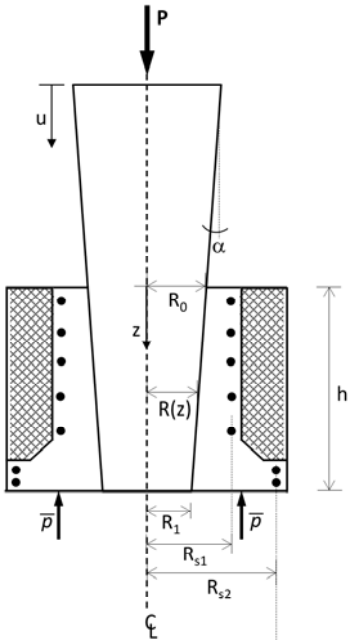

Figure 18: Longitudinal section of buffer and symbols used in model

The following relation is valid for the initial inner radius:

$$R(z) = R_0 - \tan(\alpha) \cdot z \tag{1}$$

The elastic deformation of the piston due to loading is small and it is reasonable to assume rigid body motion of the piston. Hence, when the piston is moved downwards by u, the radius $R(z)$ of the inner side of the sleeve will be increased by ΔR:

$$\Delta R(u) = \tan(\alpha) \cdot u \tag{2}$$

An expression for the *average*[2] normal strain in the tangential direction, ε_θ, at the inner side of the sleeve can now be obtained:

$$\varepsilon_\theta(u) = \frac{\Delta R(u)}{R(z)} \tag{3}$$

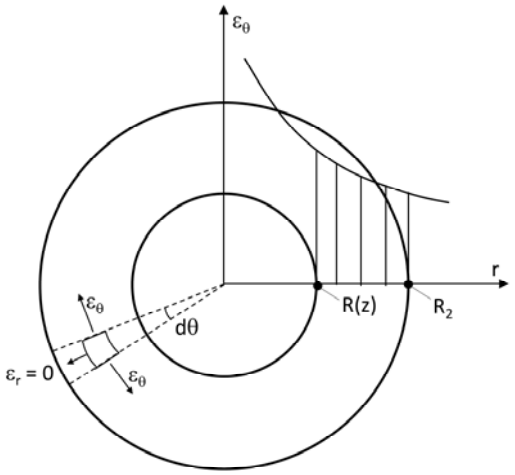

Figure 19: Schematic distribution of average normal strain, ε_θ, in tangential direction of sleeve wall

As illustrated in Figure 19, the average normal strain in the tangential direction will decrease through the wall thickness of the sleeve. Using the parameter r to describe a given point in the wall of the sleeve, we have:

$$\varepsilon_\theta(u,r) = \frac{\Delta R(u)}{r} = \tan(\alpha)\frac{u}{r}; \qquad r \in \left[R(z); R_2\right] \tag{4}$$

[2] When cracked, the average strain is taken as the sum of localized crack opening divided by the circumference

where R_2 as indicated in Fig. 19 is the initial outer radius of the effective sleeve geometry (i.e. with account for the crack inducers and therefore also varies along z).

The *average* normal strain in the stirrups can be calculated using Eq. (4) if $r = R_{s1}$ (or R_{S2}) is inserted.

The necessary kinematic relationship (Eq. 4) for the problem has now been established. This relationship will be used together with the constitutive relationships to determine the clamping force (i.e. the confinement pressure) that the sleeve is exerting on the piston as it moves downward by the magnitude u.

3.2 Constitutive relationships

3.2.1 Concrete

For the problem considered, the uniaxial tensile behavior of concrete is relevant although it only has a small impact on the overall response of the concrete buffer. It is assumed that concrete is behaving linearly elastic for normal stresses below the effective tensile strength f_{tef}, see Figure 20 (left). Young's modulus for concrete is taken as the secant modulus, which by use of the Eurocode [6] can be estimated as:

$$E_c = 22\left(\frac{f_c}{10}\right)^{0.3} \text{ (in GPa)} \tag{5}$$

where f_c (in MPa) is the mean cylinder compressive strength of concrete. The effective tensile strength, f_{tef}, is determined as

$$f_{tef} = \nu_t f_{ct} \tag{6}$$

where f_{ct} is the uniaxial tensile strength which in the following is estimated as follows, [7]:

$$f_{ct} = 0.26 f_c^{2/3} \quad ; f_c \text{ in MPa} \tag{7}$$

The effectiveness factor, ν_t, is a calibration parameter. In this investigation, a value of 0.5 (as used in other studies, see e.g. [8]) will be adopted.

Once the effective tensile strength is reached, cracking takes place. In the cracking phase, we assume a simple linear stress-crack opening relationship as shown in figure 20 (right), i.e. the tensile stress transferred across the crack is decreasing linearly and the crack is stress free when the crack width reaches w_{cr}. The same linear relationship has e.g. been used by Christiansen [8] to model tension stiffen-

ing effects in reinforced concrete bars. According to Christiansen, w_{cr} should be in the range of 0.3 – 0.4 mm. In this study, w_{cr} = 0.3mm is used.

The constitutive relationships shown in Fig. 20 can be used together with calculations of the average normal strains ε_θ, i.e. Eq. (4) to estimate the normal stresses, σ_θ, in the concrete sleeve. In a simplified but also approximated manner, the concrete stress, σ_θ, can be determined as a function of ε_θ by combining the stress-strain relationship and the stress-crack opening relationship from Fig. 20 into one single "apparent" stress-strain relationship. This approximate relationship is shown in Fig. 21, where ε_{ct} and ε_{cr} are determined as follows:

$$\varepsilon_{ct} = \frac{f_{tef}}{E_c} \tag{8}$$

$$\varepsilon_{cr}(r) = \frac{nw_{cr}}{2\pi r} \tag{9}$$

Here, n is the number of primary radial cracks. In this investigation the number of primary cracks has been taken as the number of crack inducers, i.e. n = 8.

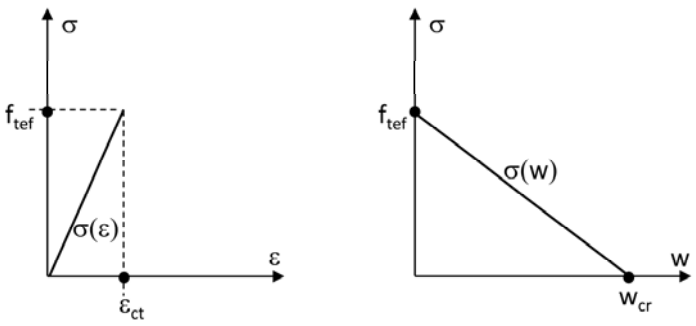

Figure 20: Assumed uniaxial tension behavior of concrete before cracking (left) and at crack development (right)

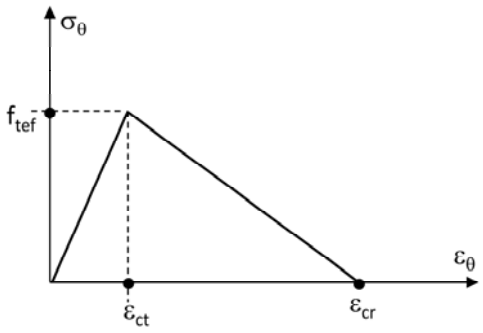

Figure 21: Simplified and approximate relation to determine normal stress, σ_θ, in concrete sleeve as function of average normal strain, ε_θ.

3.2.2 Reinforcement steel

The reinforcement is assumed to behave linearly elastic, perfectly plastic with Young modulus E_s, yield stress f_y and strain capacity ε_u. The stresses, σ_s, in the stirrups at different positions in the sleeve can then be determined as a function of the piston displacement, u. This is simply done by determining the average reinforcement strain by use of Eq. (4) with $r = R_{S1}$ and $r = R_{S2}$ and afterward inserting the average strain into the assumed elasto-plastic stress-strain relationship. Note that it is an approximation to use Eq. (4) to determine the reinforcement strain at any given point along a stirrup. In reality, the strain in each stirrup will vary depending on the distance from the point of observation to the nearest primary crack. The error introduced by this approximation primarily affects the prediction of the piston displacement, u, at which yielding of the stirrup begins. This displacement is, however, only of secondary interest since in the problem considered, the displacement at which stirrups start to yield is (and should be) much smaller than the displacement capacity, $u_{capacity}$, of the system (i.e. the piston displacement that leads to rupture of stirrups).

The average strain calculated from Eq. (4) should on the other hand not be used when it comes to estimation of the displacement capacity, $u_{capacity}$, because this may lead to unconservative results. In this case, it is necessary to take into account the variation of the strain in the stirrups which ultimately results in strain localization with some parts undergoing much larger strains than other parts. Hence, it is only the elongation of the parts that undergo much larger strains that can be taken into account when determining the deformation capacity, $u_{capacity}$. The strain localization in the rebars is caused by the bond-slip between concrete and rebars near the primary cracks. This is treated in the following.

3.2.3 Bond slip

In cracked reinforced concrete subjected to pure tension, the tensile stress in the rebars will vary between two adjacent primary cracks due to bond stresses (i.e. the shear stresses between rebar and concrete). In the vicinity of a primary crack, we

observe debonding because of the bursting stresses caused by the ribs of the rebars. The slip length (or the debonding length), l_o, depends on a number of parameters including the stress level as well as the bar diameter. An estimate of the slip length may be determine using the following equation proposed in Ref. [9]:

$$l_o = \left(1 + \frac{\sigma_s}{100}\right)\phi \qquad \leq \begin{cases} 1.3c \\ 0.65a_s \end{cases} \tag{10}$$

Here ϕ is the bar diameter, σ_s (in MPa) is the reinforcement stress in crack, c is the cover and a_s is the center distance between the reinforcement bars. For the problem studied in this paper, the two upper limits in Eq. (10) are not critical due to large covers and large distance between stirrups.

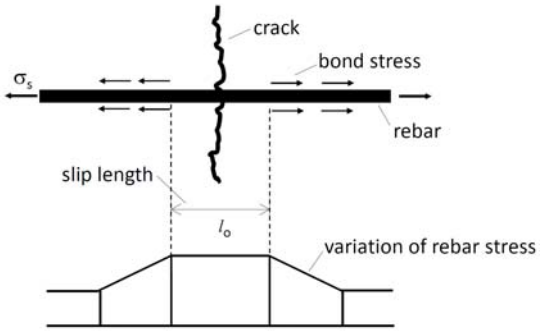

Figure 22: Schematic stress distribution in rebar at a stress free primary crack

When the crack is stress free and the bond stress outside the slip length is assumed to be uniform, we will for the rebar have the stress distribution as illustrated in Fig. 22 (see also [8]). Within the slip length, we have maximum and constant reinforcement stress. Hence, for each primary crack, we may estimate the maximum rebar elongation at failure as $l_o\varepsilon_u$, if the strains outside the slip length are neglected. Hence, if the number of primary crack is n, we find the maximum possible increase of the circumference, ΔO, of a circular stirrup as follows:

$$\Delta O = n l_o \varepsilon_u \tag{11}$$

Now, since both sides of the following equation are expressing the average elongation in the stirrup,

$$\frac{\Delta O}{2\pi R_{s1}} = \frac{\Delta R}{R_{s1}} \tag{12}$$

we can by inserting the right hand side of Eqs. (2) and (11) obtain the following estimate for the displacement capacity, u_{capacity}, of the concrete buffer:

$$u_{capacity} = \frac{n l_o \varepsilon_u}{2\pi \tan(\alpha)} \tag{13}$$

It is seen that u_{capacity} is independent of the radius of the stirrups which at first sight appears to be counter intuitive because for the same piston displacement, u, the average strain will depend on the stirrup radius (cf. Eq. 4). However, it has in the above tacitly been assumed that l_o is independent of the stirrup radius. This means that the same absolute elongation capacity, $nl_o\varepsilon_u$, is available in the stirrups irrespective of the stirrup size. Hence, the average strain capacity increases when the stirrup radius decreases. These two opposite trends compensate for the fact, that the actual strain is larger for smaller stirrup radii.

3.2.4 Interfacial shear-friction

The main load transfer mechanism in the proposed concrete friction buffer is shear-friction, which is mobilized in the interface/casting joint between the piston and the sleeve. In the present problem, the mechanical property of this interface is affected by the roughness of the piston surface as well as the wax, which was applied to the pistons in selected specimens. As mentioned, the pistons were cast in a smooth metallic form and the interface between piston and sleeve can therefore locally be classified as a smooth joint. However, it should be noted that due to production tolerances, the piston did not have a perfectly conical shape and there was to some extent ovalisation so that not all cross sections were perfectly circular. The shear capacity of a casting joint is normally determined by an empirical Coulomb type shear-friction equation:

$$\tau = c + \mu\sigma_n \tag{14}$$

where c is the cohesion and the second term is the friction contribution. The cohesion is only relevant when determining the initial static strength and will vanish once the piston begins to penetrate the sleeve. The cohesion has the useful practical application of preventing small impact forces from activating the buffer system.

When establishing a model for the load-displacement response of the concrete buffer, shear-friction is considered the main contribution. Therefore, in the following, we will not account for interfacial cohesion. Eq. (14) thus reduces to:

$$\tau = \mu\sigma_n \tag{15}$$

According to Eurocode [6], $\mu = 0.6$ for smooth joints. This value is for design purposes and therefore conservative. Based on tests, $\mu = 0.7 - 0.8$ is more suitable, [7]. For a wax treated interface, the friction coefficient is unknown.

3.3 Equilibrium conditions

The kinematic relationships and the constitutive relationships established previously allow us to determine the internal stresses in the sleeve for any given value of the piston displacement, *u*. Now, to determine the relationship between the external applied load, *P*, and the piston displacement, *u*, we need to find the relationships between the external load and the internal stresses. These relationships are established by setting up the equilibrium conditions.

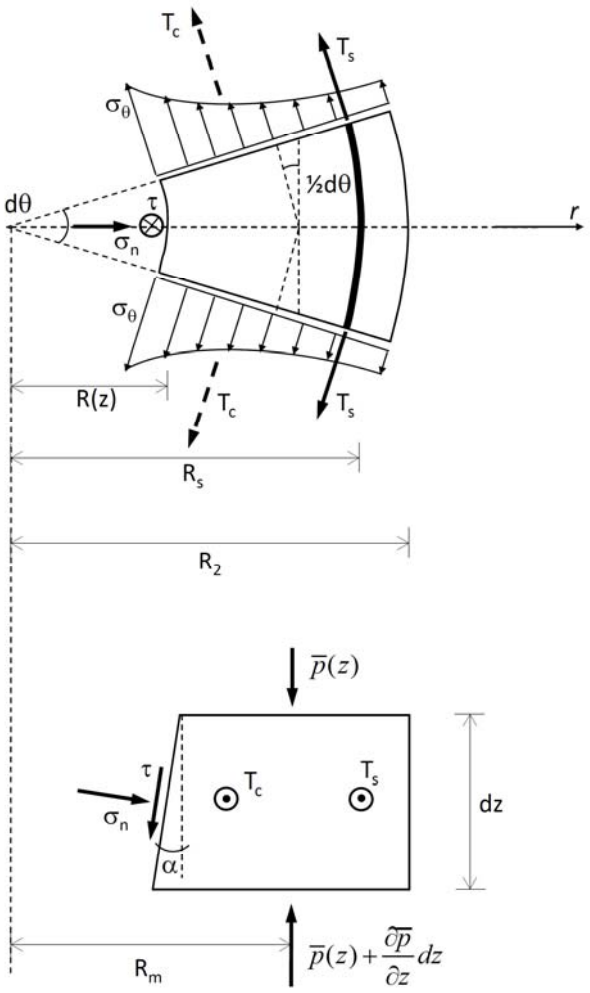

Figure 23: Free body diagram of a segment of the sleeve

With reference to the z-axis shown in Fig. 18 and the (r, θ)-system indicated in Fig. 19 we now consider a free body diagram of a segment of the sleeve confined by the angle $d\theta$ and the height dz, see Fig. 23. The interface to the piston is acted upon by a compressive normal stress, σ_n, and a shear stress, τ. At the radial boundaries of the segment, we have a distribution of tensile normal stresses in the concrete, σ_θ, which may be non-zero throughout the wall thickness (i.e. for $R(z) \leq r \leq R_2$) or only non-zero in a part of the wall depending on the level of cracking. In Fig. 23(top), a situation corresponding to un-cracked sleeve has been schematically shown. The resultant of the σ_θ-distribution over the wall thickness is denoted as T_c (i.e. a force per unit length dz). T_c has been indicated by the dashed arrow in Fig. 23(top). It is noted that T_c is a function of u and z. By combining Eq. (4) with the stress-strain relationship shown in Fig. 21, we can determine T_c from:

$$T_c(u,z) = \int_{R(z)}^{R_2} \sigma_\theta(u,r)dr \tag{16}$$

As indicated in the Fig. 23 (top), the stirrups crossing the radial boundaries carry a tensile force T_s (also a force per unit length, dz, of the sleeve height). For the geometry of the tested buffers, the position of T_s is at $R_s = R_{s1}$ or $R_s = R_{s2}$ depending on the location of the considered segment. As described previously, the stirrup stresses may be found by relating the average strain (Eq. 4) at $r = R_s$ with the assumed elasto-plastic stress-strain relationship for the rebars. Hence, T_s may be found be multiplication of the stirrup stresses with the stirrup area per unit height of the sleeve wall. It is noted that T_s is in principle also a function of both u and z since the stirrup content may vary along the sleeve height as well as the stirrup bend diameter may vary.

The total resultant, $T(u, z)$, of the normal stresses in the radial boundaries of the segment is then:

$$T(u,z) = T_c(u,z) + T_s(u,z) \tag{17}$$

At the cross sectional boundaries (i.e. the horizontal boundaries) of the segment, compressive normal stresses have to develop to equilibrate the stresses acting on the interface with the piston. In Fig. 23 (bottom), the compressive normal stresses on the cross sectional boundaries are represented by the line loads $\bar{p}(z)$. The boundary conditions of course dictate that $\bar{p}(z=0) = 0$ and the resultant of $\bar{p}(z=h)$ must equal the load, P, applied to the piston head.

From Fig. 23 (top), we find that the condition for equilibrium in the r-direction may be expressed as follows:

$$2 \cdot T(u,z)dz \cdot \sin\left(\frac{d\theta}{2}\right) = \left(\sigma_n \cos\alpha - \tau \sin\alpha\right) \cdot R(z)d\theta dz \tag{18}$$

By utilizing $\sin\left(\frac{d\theta}{2}\right) \cong \frac{d\theta}{2}$ for small angles and by replacing τ with $\mu\sigma_n$ according to Eq. (15) we find from Eq. (18):

$$\sigma_n = \frac{T(u,z)}{R(z)\left(\cos\alpha - \mu\sin\alpha\right)} \tag{19}$$

Moving on to the equilibrium condition for the z-direction and using the notations shown in Fig. 23 (bottom), the following equation can be established:

$$\left(\frac{\partial \overline{p}}{\partial z}dz\right)\cdot R_m d\theta = \left(\sigma_n \sin\alpha + \tau\cos\alpha\right)\cdot R(z)d\theta\cdot dz \tag{20}$$

The accumulated compression over the height of the sleeve is equal to the reaction at the base. Therefore, to equilibrate the total force, $P(u)$, transferred from the piston to the sleeve, the following must be fulfilled:

$$\begin{aligned} P(u) &= \int_0^{2\pi}\int_0^h \left(\frac{\partial \overline{p}}{\partial z}dz\right)\cdot R_m d\theta \\ &= \int_0^h\int_0^{2\pi}\left(\sigma_n \sin\alpha + \tau\cos\alpha\right)\cdot R(z)d\theta\cdot dz \end{aligned} \tag{21}$$

As can be seen, the relation in Eq. (20) has been utilized when formulating Eq. (21). Now, by replacing τ with $\mu\sigma_n$ and expressing σ_n through the right hand side of Eq. (19) we finally arrive at the following equation to determine the load-displacement response of the concrete friction buffer:

$$P(u) = 2\pi\frac{\sin\alpha + \mu\cos\alpha}{\cos\alpha - \mu\sin\alpha}\int_0^h T(u,z)dz \tag{22}$$

Expression (22) can be simplified further when the angle α defining the conical shape of the piston is small. In that case, we have:

$$P(u) = 2\pi\frac{\alpha + \mu}{1 - \mu\alpha}\int_0^h T(u,z)dz \quad \text{(for small angles } \alpha\text{)} \tag{23}$$

In a design situation, Eq. (23) can be used to determine the load carrying capacity, P_{max}, of the buffer. At the ultimate load where the tensile strength of concrete has vanished, the integral $\int_0^h T(u,z)dz$ will simply be equal to the yield capacity of all the stirrup legs crossing the longitudinal section of a sleeve wall. Hence:

$$P_{\max} = 2\pi \frac{\alpha + \mu}{1 - \mu\alpha} n_s A_s f_y \tag{24}$$

where n_s is the number of stirrups in the sleeve, A_s is the cross sectional area of one stirrup leg and f_y is the yield stress of the stirrups.

Since the buffer should be designed to have a displacement capacity that is significantly larger than the displacement needed to obtain first yielding in the stirrups, a simplified rigid-plastic behavior can be assumed when carrying out preliminary design. This means that the energy dissipation capacity of a buffer can be estimated as $W_{\text{dissipation}} = P_{\max} u_{\text{capacity}}$. Inserting the right hand side of Eqs. (13) and (24), we find:

$$W_{dissipation} = n l_o \varepsilon_u \frac{\alpha + \mu}{(1 - \mu\alpha)\alpha} n_s A_s f_y \tag{25}$$

This formula can be used to find a first estimate of the number of buffers needed to withstand a ship impact with known impact energy. Of course, $\alpha = 0$ cannot be used as explained below.

3.4 Parameter study

It appears that α, the angle of inclination of the conical surface, plays a very important role for the load carrying capacity as well as the displacement capacity, cf. Eqs. (13) and (24). It is important to note that these Equations become invalid when $\alpha \rightarrow 0$ (i.e. when the conical piston turns into a cylindrical piston). The reason is, of course, that we cannot have expansion of the sleeve when $\alpha = 0$. Hence, the stirrups cannot be activated which means that there is no resulting clamping force to mobilize friction at the interface.

In Fig. 24, load-displacement curves have been calculated by use of the model described in this section. The only parameter that has been varied is the angle α. As input for these calculations, the layout of test specimen 1-L-D has been used (although all stirrups have been given the same bend diameter D =550 mm). Further, the following parameters have been assumed: f_c = 50 MPa, f_y = 600 MPa, E_s = 200 GPa, ε_u = 8%, ν_t =0.5 w_{cr} = 0.3 mm, n = 8 and μ = 0.75.

As can be seen in Fig. 24, only a small variation in the load carrying capacity is found for the interval of α considered. However, the point at which the stirrups begin to yield is delayed as α becomes smaller. Most significant is the change in the displacement capacity. Smaller values of α mean that the rate of expansion decreases and a much larger displacement, u, has to take place before the stirrups rupture. It is important to note that there is most likely a lower limit for α (differ-

ent from zero), below which calculations according to the presented model will no longer be valid. The lower limit can only be determined by means of experiments.

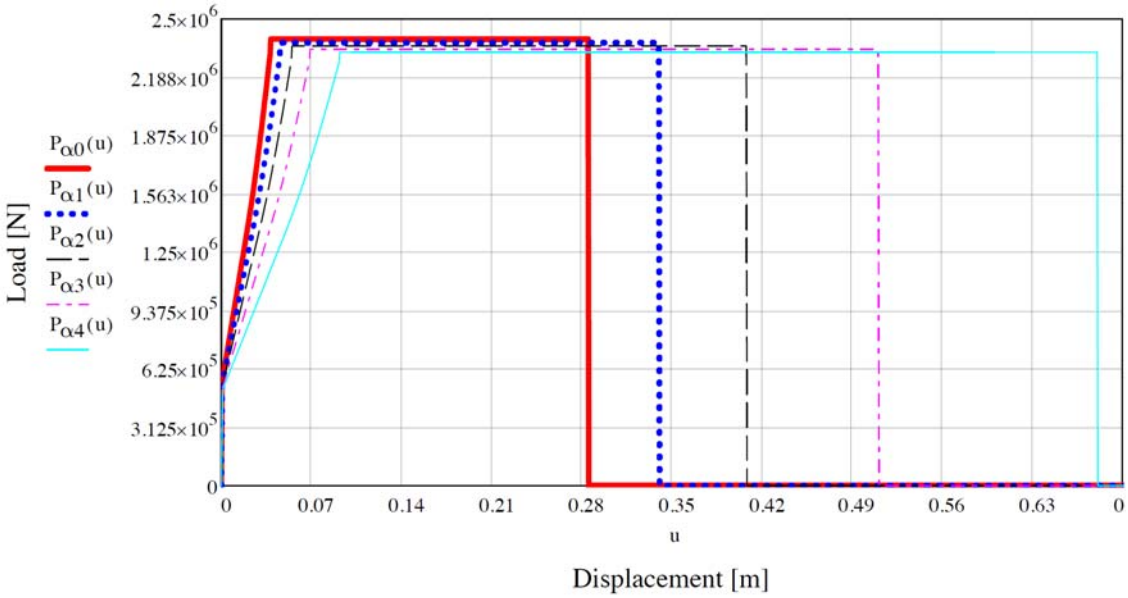

Figure 24: Calculated load-displacement curves for different generatrix inclination, $\alpha_0 = 1.46^o$; $\alpha_1 = 1.2^o$; $\alpha_2 = 1.0^o$; $\alpha_3 = 0.8^o$; $\alpha_4 = 0.6^o$.

4 Comparison of tests with model

4.1 Model parameters

In the following, the established model will be compared to experimental results. The tested material parameters which are used (directly or indirectly) in the model are: f_c, f_u, E_s and ε_u. As the uniaxial compression strength of concrete, an average value of f_c = 52.2 MPa found from cylinder tests has been used. Based on the compressive strength, the Young modulus and the tensile strength of concrete have been estimated according to the equations provided in Section 3.2. Based on average results of uniaxial tension tests of rebars, the following values have been used to describe the reinforcement behavior: $f_y = f_u$ = 606.2 MPa, E_s = 195.5 GPa and ε_u = 7.75%. The assumption of $f_y = f_u$ means that the elasto-plastic stress-strain relationship assumed for the stirrups will represent and upper envelope for the actual stress-strain behavior shown in Fig. 10.

Besides of the tested material properties, the model also requires four other parameters, which need to be estimated or assumed. These are:

- The effectiveness factor, ν_t, for concrete in tension. As mentioned in Section 3.2, a value of 0.5 is often used in the literature. The same value is adopted here.

- The crack width, w_{cr}, at which the crack becomes stress free. The value of this parameter is closely linked to the assumed linear softening curve and the effective tensile strength (Fig. 20). Christiansen [8] suggested that w_{cr} should be in the interval 0.3 - 0.4 mm. In the following a constant value of 0.3 mm is adopted.

- The number of primary cracks, n. In the tested buffers, we have cast in eight crack inducers which locally reduced the sleeve wall thickness by approximately 50% and thereby functioned as notches at which cracks initiated. Therefore, n = 8 has been adopted when using the model. For general applications where crack inducers are not cast in, estimates of the crack spacing and thereby n may be carried out by use of a suitable model proposed in the literature (e.g. [8]). It should, however, be noted that using a model for linear members loaded in tension will not necessarily lead to accurate estimates of the crack spacing for problems of the type considered in this paper because tensioned circular stirrups (due to expansion) generate radial compression on the concrete.

- The friction coefficient, μ. This value is in this study considered as a calibration parameter which is used obtain agreement between tested load carrying capacity and modelled load carrying capacity (i.e. the horizontal plateau of the response curve). There are several reasons why it is difficult to make an independent qualified estimate for μ. As mentioned, even though the interface between piston and sleeve can be classified as a "smooth joint", there is also the effect of production tolerances, which means that a perfectly conical shape has not been obtained. Ovalisation of the piston cross sections obviously affects the apparent friction coefficient. Finally, for the specimens with wax treated interface, there is a reduced friction coefficient.

4.2 Results for specimens with low stirrup content

Fig. 25 shows the predicted response for test specimens 1-L-D, 2-L-D and 3-L-W. To obtain agreement between tested load-carrying capacity and model, the friction coefficient has been assumed as $\mu = 0.85$ for specimens 1-L-D and 2-L-D while for specimens 3-L-W with wax on the interface, $\mu = 0.56$ has been adopted. The full response has been depicted, i.e. the calculations have been depicted for piston displacement, u, up to $u_{capacity}$, where $u_{capacity} \sim 250$ mm has been estimated using Eq. (13). It can be seen that the model prediction agrees fairly well with experiments. It is especially interesting to note that even though μ is calibrated only to obtain agreement with the ultimate load, then the adopted value of μ also leads to reasonable predictions of the ascending part of the response curve. The first portion of the ascending part has been enlarged and shown in Figure 26. In relation to the ascending part, it should be noted that just before the transition to the horizontal plateau (see Fig. 25 at displacement u between 25 – 50 mm) there is a loss of stiffness (i.e. the gradient of the ascending curve decreases). The reason for this detail can be found in the two different diameters of the stirrups. First, the stirrups with D = 550 mm start to yield. Then, when the displacement increases further, the stirrups with D = 700 mm placed at the bottom of the sleeve begin to yield as well resulting in the horizontal plateau.

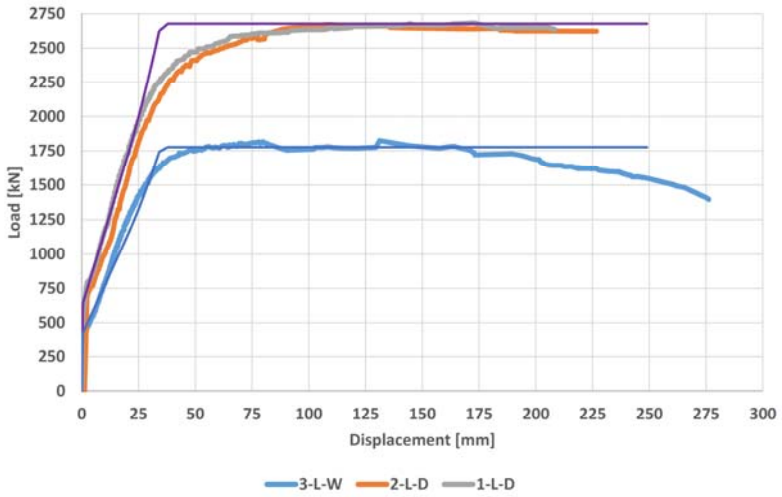

Figure 25: Calculated load-displacement response compared with tests, specimens with low stirrup content

A friction coefficient of 0.85 exceeds typical values of 0.70 – 0.80, which is the usual interval found from tests with smooth casting joints. The above mentioned production tolerances leading to a non-perfect conical shape for the pistons likely result in a higher friction coefficient. Regarding the lower friction coefficient, $\mu = 0.56$, a discussion will be provided in relation to comparison with test 6-H-W.

To model the smooth transition from the ascending part of the response curve to the yield plateau as observed in tests, calculations have also been carried out using the "true" stress-strain relationship for the reinforcement. That is, instead of using an idealized elasto-plastic stress-strain relationship, the true stress-strain curve obtained from tension tests (see Fig. 10) has been used in this more refined model. The calculations for this case can be seen in Fig. 27. All other parameters are the same as those used when determining the results in Fig. 25. It appears that by using the true stress-strain relationship for the reinforcement, we find better predictions of the behavior of specimen 1-L-D and 2-L-D. The agreement between model and experiment is on the other hand less impressive for specimen 3-L-W.

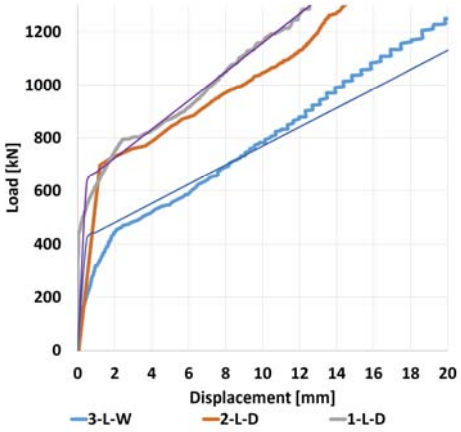

Figure 26: Ascending part of calculated and tested load-displacement response for specimens with low stirrup content

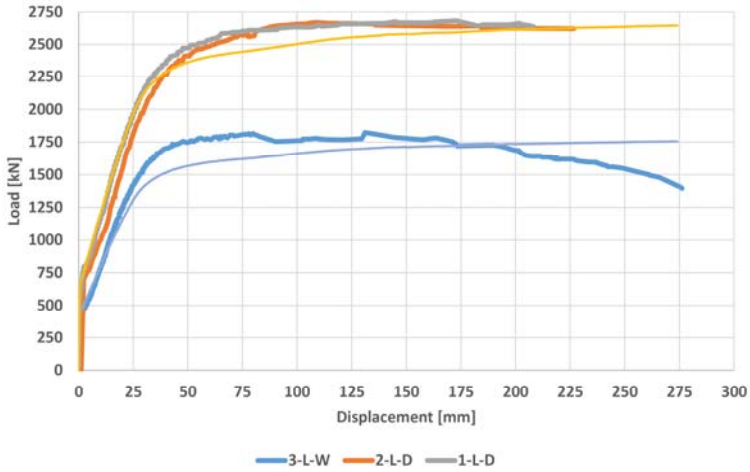

Figure 27: Calculated load-displacement response by use of true stress-strain relationship for reinforcement

4.3 Results for specimens with high stirrup content

As described in the Chapter 2, the piston of specimens 4-H-D and 5-H-D failed by crushing at an early stage where the stirrups in the sleeves were still in the elastic range. The results of these tests are therefore of less interest. Only for specimen 6-H-W with high stirrup content, the test was completed with rupture of stirrups. As mentioned, however, only a portion of the horizontal plateau was determined because the LVDTs were removed before end of testing. Fig. 28 shows the model prediction compared with the test. In the calculations, we have used the same parameters as those applied to specimen 3-L-W. The only difference here is the higher stirrup content. It is interesting to note that a close prediction of the load

carrying capacity has been obtained using the same low friction coefficient μ = 0.56 as that adopted for specimen 3-L-W. It seems therefore reasonable to conclude that μ = 0.56 is a fair estimate of the friction coefficient for a smooth and wax treated interface. From Fig. 28, it is noted that the ascending branch is also captured fairly well by the model. The estimated displacement capacity in this case, $u_{\text{capacity}} \sim 330$ mm, should not be compared with the end point on the experimental response curve due to the reasons mentioned above.

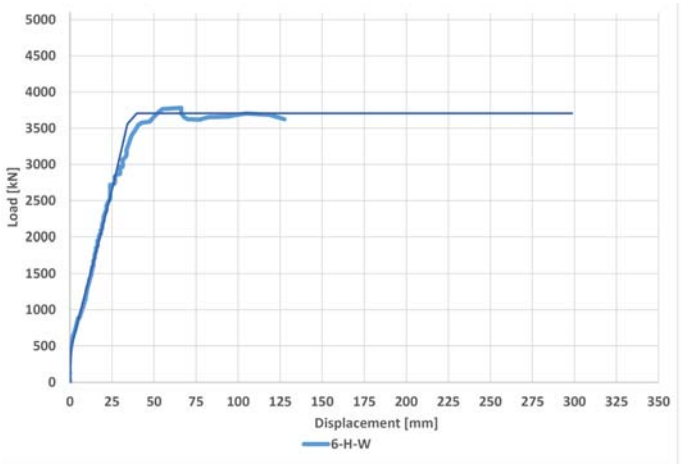

Figure 28: Calculated and tested load-displacement response for specimen 6-H-W

5 Discussions and Conclusions

In this paper, a mechanical system to protect bridge piers from ship impact has been conceptually introduced, experimentally evaluated and analytically modelled. The system is based on Concrete Friction Buffers that can be directly installed on new or existing foundation structures of bridges. The buffer consists of a conical concrete piston surrounded by a reinforced concrete sleeve, which it penetrates upon impact of a vessel, thereby deforming the device and dissipating energy to reduce the forces acting on the foundation structure. The concept is in principle applicable to all accidental loads, be it a derailed train, vehicle impact or any other accidental impact necessary to consider in design.

The working principle of this impact protection system has been experimentally demonstrated and evaluated by testing six prototype specimens with a variety of design parameters including the reinforcement ratio and the frictional property of the interface between piston and sleeve. Based on experimental data and observations of the deformation behavior of the system under load, an analytical model has been established to predict the load-deformation behavior of the system including maximum expected load level, displacement capacity and energy absorption capacity. The established model compares well with the obtained experimental data and may serve as a basis for a design tool for the protection device.

Acknowledgements

The authors would like to thank EXPAN for their help with producing the test specimens and COWI A/S for their financial support without which this work would not have been made possible.

6 References

[1] European Committee for Standardization (CEN). EN-1991-1-7, Eurocode 1, Action on structures, Part 1-7: General actions – Accidental load. CEN, Brussel, 2006

[2] American Association of State Highway and Transportation Officials (AASTHO). *Guide Specifications and Commentary for Vessel Collision Design of Highway Bridges*. 2nd ed. American Association of State Highway and Transportation Officials, Washington DC, 2009

[3] Hoang LC, Lützen M. Ship collisions with pile supported structures – Estimates of strength and ductility requirements. *Structural Engineering International*, Vol. 22, No. 3, 359-364, 2012

[4] Larsen, OD. *Ship Collision with Bridges – The Interaction between Vessel Traffic and Bridge Structures*. Structural Engineering Documents 4, IABSE, Zürich, 1993

[5] Bennedsen A, Østerby I. *Protection of bridge piers from ship collision through concrete buffers*. B. Eng. Thesis. Department of Civil Engineering, Technical University of Denmark, 2015

[6] European Committee for Standardization (CEN). EN-1992-1-1, Eurocode 2, Design of Concrete structures - Part 1-1: General rules and rules for buildings. CEN: Brussel, 2008

[7] Nielsen MP, Hoang LC. *Limit Analysis and Concrete Plasticity*, 3rd edition, CRC-Press, 818 pp, 2011

[8] Christiansen MB. *Serviceability Limit State Analysis of Reinforced Concrete*. Department of Civil Engineering, Technical University of Denmark, 2000

[9] Olsen DH, Nielsen MP. *Ny teori til bestemmelse af revneafstande og revnevidder i betonkonstruktioner* [*New theory for crack width design in concrete structures*]. Department of Structural Engineering, Technical University of Denmark, Report No. R-254, 1990

DANSK SELSKAB FOR BYGNINGSSTATIK

Anmodning om optagelse i selskabet indsendes til et af bestyrelsens medlemmer:

Henrik Elgaard Jensen (formand), Tlf. 51 61 10 00
Rambøll, Hannemanns Allé 53, 2300 København S

Niels Højgaard Pedersen (sekretær), Tlf. 72 44 75 34
Vejdirektoratet, Guldalderen 12, 2640 Hedehusene

Klaus Lynggaard (kasserer), Tlf. 22 70 96 30
MT Højgaard A/S, Knud Højgaards Vej 9, 2860 Søborg

Linh Cao Hoang, Tlf. 45 25 17 06
DTU Byg, Brovej, 2800 Kgs. Lyngby

Srirengan Thangarajah, Tlf. 29 40 32 19
Per Aarsleff A/S

Thomas Hansen, Tlf. 88 19 10 00
ALECTIA A/S, Teknikerbyen 34, 2830 Virum

Carsten Munk Plum, Tlf. 45 66 10 11
ES-Consult A/S, Sortemosevej 19, 3450 Allerød

Lars Krog Christensen, Tlf. 70 12 24 00
MT Højgaard, Knud Højgaards Vej 9, 2860 Søborg

Selskabets formål er at arbejde for den videnskabelige udvikling af bygningsmekanikken - både teori for og konstruktion af alle slags bærende konstruktioner - fremme interessen for faget, virke for et kollegialt forhold mellem dets udøvere og hævde dets betydning overfor og i samarbejde med andre grene af ingeniørvidenskaben. Formålet søges bl.a. realiseret gennem møder med foredrag og diskussioner samt gennem udgivelse af "Bygningsstatiske Meddelelser".

Som medlemmer kan optages personlige medlemmer, firmaer og institutioner, som er særligt interesserede i bygningsmekanik, eller hvis virksomhed falder indenfor bygningsmekanikkens område.

Det årlige kontingent er for personlige medlemmer 300 kr., for firmaer samt institutioner 1.800 kr. Studerende ved Danmarks Tekniske Universitet og andre danske ingeniørskoler samt indtil 2-års kandidater kan optages som juniormedlemmer uden stemmeret for et årskontingent på 80 kr. Pensionerede medlemmer med mindst 10 års medlemsanciennitet kan opnå status som pensionistmedlem med stemmeret for et årskontingent på 100 kr.

Selskabets medlemmer modtager frit "Bygningsstatiske Meddelelser", der udsendes kvartalsvis. Endvidere publiceres "Bygningsstatiske Meddelelser" på Selskabets hjemmeside www.dsby.dk. Manuskripter til optagelse i "Bygningsstatiske Meddelelser" modtages af redaktøren.